ACS APPLIED MATERIALS & INTERFACES

Letter

www.acsami.org

Crystalline Mesoporous $K_{2-x}Mn_8O_{16}$ and ε-MnO_2 by Mild Transformations of Amorphous Mesoporous Manganese Oxides and Their Enhanced Redox Properties

Altug S. Poyraz,[†] Wenqiao Song,[†] David Kriz,[†] Chung-Hao Kuo,[†] Mohammad S. Seraji,[†] and Steven L. Suib*[,‡]

[†]Department of Chemistry and [‡]Department of Chemistry Institute of Materials Science, University of Connecticut, U-3060, 55 North Eagleville Road, Storrs, Connecticut 06269, United States

S *Supporting Information*

ABSTRACT: Synthesis of crystalline mesoporous $K_{2-x}Mn_8O_{16}$ (Meso-OMS-2), and ε-MnO_2 (Meso-ε-MnO_2) is reported. The synthesis is based on the transformation of amorphous mesoporous manganese oxide (Meso-Mn-A) under mild conditions: aqueous acidic solutions (0.5 M H^+ and 0.5 M K^+), at low temperatures (70 °C), and short times (2 h). Meso-OMS-2 and Meso-ε-MnO_2 maintain regular mesoporosity (4.8–5.6 nm) and high surface areas (as high as 277 m^2/g). The synthesized mesoporous manganese oxides demonstrated enhanced redox (H_2-TPR) and catalytic performances (CO oxidation) compared to nonporous analogues. The order of reducibility and enhanced catalytic performance of the samples is Commercial-Mn_2O_3 < nonporous-OMS-2 < Meso-Mn_2O_3 < Meso-OMS-2 < Meso-ε-MnO_2 < Meso-Mn-A.

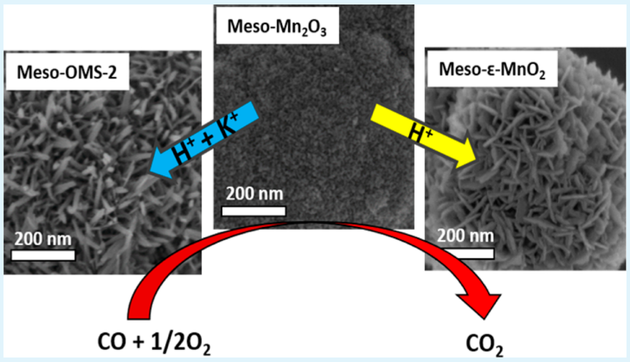

KEYWORDS: *mesoporous, OMS-2, ε-MnO2, manganese oxide, CO oxidation, UCT mesoporous materials*

Nanocrystalline and monomodal pore size multivalent mesoporous transition metal oxides (MTMOs) have attracted much attention in the past two decades and have been the subject of thousands of research studies. The interest in multivalent MTMOs originates from their catalytic, electronic, sorption, and magnetic properties which are superior to those of their nonporous counterparts.[1−9] However, because of synthetic limitations in the sol−gel chemistry of TMs, multivalent MTMOs (i.e., Fe, Mn, and Co) can be synthesized only with a limited (usually one) number of crystal phases.[2,4,7,10−14] That limits the potential use of mesoporous MTMOs for various applications, because their versatility arises from the numerous oxide structures, polymorphs, and stable oxidation states.[15−21] The situation is more complicated for manganese oxides. In addition to thermodynamically stable major Mn_2O_3 (Bixybyite, Mn = 3^+), Mn_3O_4 (Hausmannite, Mn = 2^+ & 3^+), and β-MnO_2 (Mn = 4^+) phases, there are many other oxide structures (i.e., Mn_5O_8 & MnO), polymorphs of MnO_2 (α-, β-, γ-, δ-, ε-, and λ-), and cation-stabilized octahedral coordinated microporous manganese oxides (octahedral molecular sieves, OMS).[22−25] Thus far, ordered mesoporous manganese oxides have only been synthesized with Mn_2O_3 (Bixbyite) or Mn_3O_4 (Hausmannite) phases by direct sol−gel methods.[2,12] Other phases such as $K_{2-x}Mn_8O_{16}$ (Cryptomalene) and γ-MnO_2 have only been obtained using a hard template (nanocasting) such as mesoporous silica (i.e., SBA-16 and KIT-6).[26] This approach requires subsequent template removal by NaOH following the formation of the desired oxide structure.

Here, we are reporting the transformation of mesoporous amorphous manganese oxide (Meso-Mn-A) to crystalline mesoporous Mn_2O_3 (Meso-Mn_2O_3), ε-MnO_2 (Meso-ε-MnO_2), and K_{2-x}-Mn_8O_{16} (Meso-OMS-2) materials by preserving the mesoporosity under mild (0.2−0.5 M H^+ & 40−70 °C) conditions. Scheme 1 summarizes the transformation conditions for the materials mentioned in this manuscript (see the Supporting Information for detailed experimental procedures). The amorphous manganese oxide (Meso-Mn) was synthesized using a recently developed inverse micelle templating route. This method uses inverse nonionic surfactant micelles (P123) as a soft template, whereas the sol−gel process of manganese sols is controlled in acidic media (HNO_3) by NOx chemistry. The Meso-Mn was subjected to a heating cycle of 150 °C (10 h) + 250 °C (3 h) + 350 °C (2 h) to form amorphous Meso-Mn-A. Meso-Mn-A was used as a substrate to form other crystalline mesoporous manganese oxides: (1) Meso-Mn_2O_3 was formed by heating Meso-Mn-A at 450 °C for 1 h, (2) Meso-ε-MnO_2 was synthesized by treating

Received: May 9, 2014
Accepted: June 27, 2014
Published: June 27, 2014

Scheme 1. Schematic Illustration of the Synthetic Approach to Form Crystalline Mesoporous Manganese Oxides

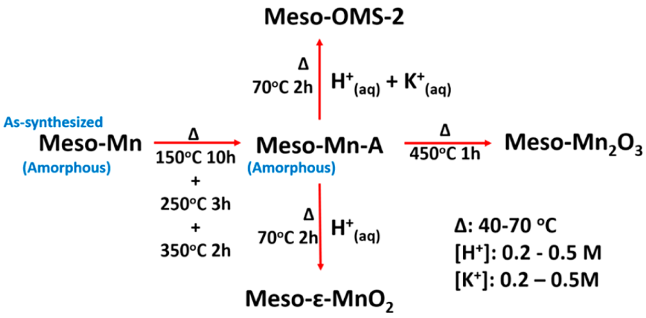

Meso-Mn-A in a 0.5 M aqueous sulfuric acid solution at 70 °C for 2 h, and (3) Meso-OMS-2 was synthesized by treating Meso-Mn-A in a 0.5 M aqueous sulfuric acid solution containing 0.5 M KCl at 70 °C for 2 h.

These materials are members of the recently discovered University of Connecticut (UCT) mesoporous materials family. The UCT materials are randomly packed monodisperse nanoparticle aggregates and the mesopores are continuous intraparticle voids. The UCT materials typically have one low-angle diffraction line indicating the size of the building blocks (nanoparticles) and a Type IV adsorption isotherm indicating a regular mesoporous structure.[2] Figure S1a in the Supporting Information shows the low-angle PXRD patterns of the mesoporous samples. All samples have one low-angle diffraction line indicating the existence of a mesostructure. The positions of the diffraction lines are at around ~8 nm for all the mesoporous samples except for Meso-Mn_2O_3 (10.8 nm) (see Table 1). The increase is attributed to a unit-cell expansion upon heat treatment caused by nanoparticle sintering, which is also typical for UCT materials.[2,27]Figure S1b in the Supporting Information shows the wide-angle PXRD patterns of mesoporous manganese oxides. Meso-Mn-A does not show any diffraction lines (amorphous) whereas Meso-Mn_2O_3 shows the bixbyite (Mn_2O_3) crystal structure with a crystallite size of 11.8 nm (Table 1). Acid treatment of the Meso-Mn-A sample yielded the ε-MnO_2 (Meso-ε-MnO_2) phase with a crystallite size of 2.3 nm (see Figure S1b in the Supporting Information and Table 1). The ε-MnO_2 (Akhtenskite) is a relatively less known phase of manganese oxide and is structurally (and electrochemically) very similar to the γ-MnO_2 phase.[23,24] Both (ε- and γ-) consist of an intergrowth 1 × 1 pyrolusite (2.3 Å × 2.3 Å) and 2 × 1 ramsdellite (4.6 Å × 2.3 Å) phases. However, the ε- phase shows more structural faults (De Wolff faults) and microtwinning than the γ- phase.[23] MnO_6 octahedral units are the building blocks of ε-MnO_2 as well as numerous other microporous manganese oxides known as Octahedral Molecular Sieves (OMS). The micropores of OMS materials are occupied with charge balancing cations (i.e., H^+, K^+, Ag^+, Rb^+, Mg^{2+}, Ba^{2+}) and manganese is mix-valent with oxidation states of 2^+, 3^+, and 4^+.[16,25,28] Among the OMS materials, potassium containing manganese oxide octahedral molecular sieves (K-OMS-2) has attracted much of the interest because of its advanced redox activity in catalytic reactions.[17,19,29,30] OMS-2 is synthetic analogue of a naturally occurring microporous manganese oxide mineral, cryptomelane (4.7 Å × 4.7 Å).[27] Synthesized mesoporous K-OMS-2 (Meso-OMS-2) is the cryptomelane ($K_{2-x}Mn_8O_{16}$) phase with a crystallite size of 5.0 nm (see Figure S1b in the Supporting Information and Table 1). Figure S1 in the Supporting Information shows the N_2 sorption isotherms (c) and BJH desorption pore size distributions (d) of mesoporous manganese oxides. BET surface areas, pore sizes, and pore volumes of mesoporous manganese oxides are summarized in Table 1. Regardless of applied heat or acid treatments, all the materials have a Type IV adsorption isotherm indicating the existence of mesopores followed by a Type I hysteresis loop suggesting a regular mesoporosity. Acid-treated samples exhibit higher mesopore sizes than the parent Meso-Mn-A (3.4 nm) and Meso-Mn_2O_3 (3.8 nm) with Meso-ε-MnO_2 having the largest pore size (5.6 nm). In addition, all mesoporous samples exhibit high BET surface areas (>128 m^2/g) where Meso-OMS-2 is the one with the highest surface area (277 m^2/g). For comparison, commercial Mn_2O_3 (C−Mn_2O_3) and nonporous K-OMS-2 synthesized by reflux methods (R-OMS-2) were also analyzed. Their physicochemical properties are summarized in Table 1 and Figure S2 in the Supporting Information. Both C−Mn_2O_3 and R-OMS-2 do not have any low-angle diffraction lines (see Figure S2a in the Supporting Information) and have high crystallinity (see Figure S2b in the Supporting Information and Table 1). They also demonstrate a Type III adsorption isotherm due to their nonporous nature (see Figure S2c in the Supporting Information), and therefore they exhibit low BET surface areas (<56 m^2/g).

Transformation of Mn_2O_3 and Mn_3O_4 phases to MnO_2 in acidic aqueous solutions relies on dissolution-disproportion reactions (see equations S1−S3 in the Supporting Information).[31,32] Mn^{3+} in the solid is reduced to Mn^{2+} which leaches out from the oxide surface (Mn^{2+} (aq)); meanwhile Mn^{3+} in the solid is oxidized to Mn^{4+} to form MnO_2 in acidic aqueous media. Sinha et al. converted a mesoporous mixed phase

Table 1. Structural Parameters of Mesoporous Manganese Oxide Samples and Their Catalytic Performances for CO Oxidation

sample ID	low-angle PXRD peak position(nm)	surface area S_{BET} (m^2/g)	BJH des. pore size (nm)	BJH ads. pore size (nm)	pore volume (cc/g)	Scherrer crystal size (nm)	crystal structure	T_{100}[a] (°C)
Meso-Mn-A	7.9	238	3.4	3.8	0.31	NA	NA	25
Meso-Mn_2O_3	10.8	128	3.8	4.9	0.22	11.8	Mn_2O_3 (Bixbyite)	50
Meso-ε-MnO_2	8.4	196	5.6	5.2	0.32	2.3	ε-MnO_2 (Akhtenskite)	50
Meso-OMS-2	8.2	277	4.8	6.7	0.48	5.0	$K_{2-x}Mn_8O_{16}$ (Cryptomelane)	50
C-Mn_2O_3	NA	9	NA	NA	0.01	34.6	Mn_2O_3 (Bixbyite)	NA
R-OMS-2	NA	56	NA	NA	0.69	8.6	$K_{2-x}Mn_8O_{16}$ (Cryptomelane)	225

[a] T_{100} is 100% conversion temperatures in CO oxidation experiments. The conversion is based on CO. 1%CO + 2% O_2 were diluted in N_2. The flow rate was 15 cc/min. The experiments were done at atmospheric pressure.

(Mn_3O_4 and Mn_2O_3) manganese oxide to γ-MnO_2 using a 10 M sulfuric acid solution at RT (20x more concentrated than the conditions used in this study).[11,33] In another study, Walanda et al. transformed nonporous Mn_2O_3 to γ-MnO_2 (0.5 M H^+, 80 °C for 1 week) and OMS-2 (5.0 M H^+, 80 °C for 1 week) by sulfuric acid treatment.[32] Because of the nanoparticle nature of UCT materials, the transformation conditions are much milder (0.5 M H^+ at 70 °C for 2 h) and resulting materials exhibit high surfaces area and mesoporosity. In addition, mesoporous ε-MnO_2 and OMS-2 have not been observed previously. To validate the mildness of the reaction conditions, commercial Mn_2O_3 (C−Mn_2O_3) was treated with 0.5 M sulfuric acid solution at 80 °C for 4 h. Despite the transformation being done at a higher temperature (70 °C vs 80 °C) and longer time (2 h vs 4 h), the transformation was incomplete and the major crystalline phase was still Mn_2O_3 (see Figure S3 in the Supporting Information). Most probably, the transformation only occurred on the surface and the bulk remained the same.

Morphology studies using SEM (Figure 1 and Figure S4 in the Supporting Information) revealed that the acid treatment caused drastic changes on the surface morphology of mesoporous manganese oxides, despite the low magnification images showing aggregated micron sized spheres for all samples. Direct heat treatment of Meso-Mn-A to form Meso-Mn_2O_3 did not cause a significant change in the surface morphology. The sample preserved its relatively smooth surface morphology and one can realize textural porosity on the particle surfaces (compare Figure S4 in the Supporting Information and Figure 1a). However, the surface morphology of Meso-ε-MnO_2 particles show flakes growing out the particles with wide openings (Figure 1b) and Meso-OMS-2 sample has surfaces covered by needles growing out the spherical particles (Figure 1c). Surface morphologies like fibers, needles, flakes, nanoplates, and nanorods have widely been observed for tunnel structured MnO_2 (OMS) materials.[15,18,23,25,28,30] However, these materials failed to demonstrate regular, monomodal porosity as evidenced by the lack of a Type IV N_2 adsorption isotherm. Therefore, HR-TEM images of mesoporous manganese oxide samples were also collected for better evaluation of the changes of surface morphologies and the origins of mesoporosity (Figure 2 andFigure S5 in the Supporting Information). HR-TEM images of Meso-Mn-A and Meso-Mn_2O_3 samples show nanoparticle aggregates with a porous nature formed by intraparticle voids (mesopores) (Figure 2a, b). Unlike Meso-Mn_2O_3 sample, the origin of mesoporosity is not clear for Meso-ε-MnO_2 and Meso-OMS-2 samples because of the sample thickness. HR-TEM images of Meso-ε-MnO_2 (Figure 2c) and Meso-OMS-2 (Figure 2d) show flakes and needles growing on the surface of particles, which is consistent with the SEM analyses. Probably, interior of these materials still preserve the nanoparticle aggregate nature after transformation so as the mesoporosity. More detailed HR-TEM analyses using the samples prepared by focus ion beam (FIB) is underway for Meso-ε-MnO_2 and Meso-OMS-2 samples to investigate the origins of mesoporosity in Meso-ε-MnO_2 and Meso-OMS-2 samples.

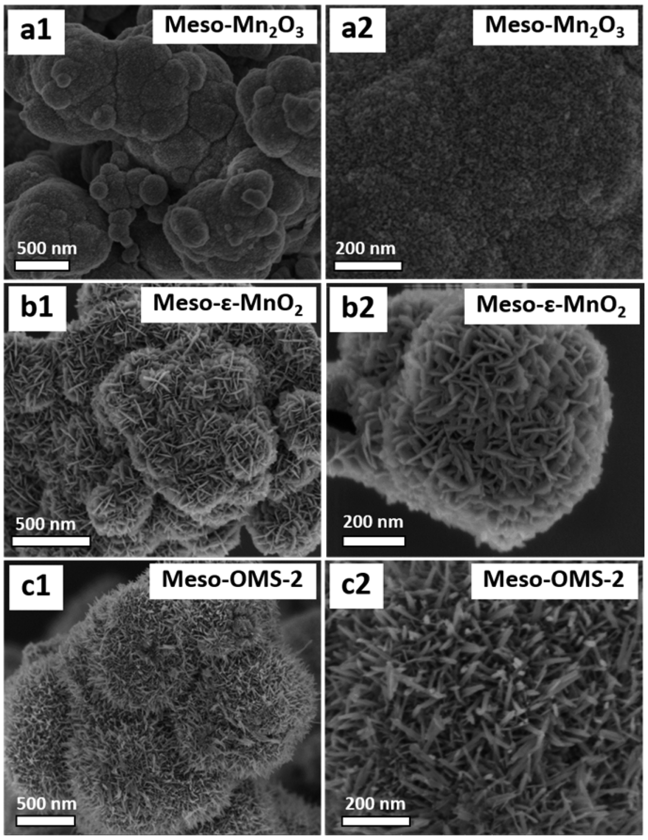

Figure 1. SEM images of mesoporous manganese oxides (a) Meso-Mn_2O_3 (scale bars are 500 nm at a1 and 200 nm at a2), (b) Meso-ε-MnO_2 (scale bars are 500 nm at b1 and 200 nm at b2), and (c) Meso-OMS-2 (scale bars are 500 nm at c1 and 200 nm at c2).

As redox catalysts, manganese oxides are known to be very active for selective or total oxidations or oxidative transformations of various organic compounds in both liquid and gas phase reactions.[15,19,29,30,33] High-surface-area, nanocrystalline manganese oxides with readily interchangeable multiple oxidations states are found to be the most active in these studies, because the heterogeneous catalytic reactions occur on the catalyst surface. From a pure redox activity perspective; more readily reduced surface species generally have higher redox activity, because their reduction generally occurs at lower temperatures.[35] The redox properties of mesoporous manganese oxides were examined by H_2-TPR (Figure 3a). Among all the mesoporous samples, Meso-Mn-A showed the lowest reduction temperature of 318 °C with a two-step reduction (the second is at 469 °C). Meso-Mn_2O_3 was reduced in one step with a peak position of 502 °C which was lower than the commercial analogue (C-Mn_2O_3, 534 °C). The shift of the reduction temperature was attributed to the more easily reducible nature of nanocrystalline Meso-Mn_2O_3. Meso-OMS-2 showed a two-step reduction (at 347 and 411 °C) and the ratio of the lower temperature peak to the higher temperature peak was around 1. Therefore, the lower temperature reduction was attributed to the reduction of MnO_2 to Mn_2O_3 and the higher temperature peak was attributed to the reduction of Mn_2O_3 to MnO. On the other hand, R-OMS-2 (nonporous) only showed one broad reduction peak centered at 418 °C, which is typical for large and nonporous particles.[34] Meso-ε-MnO_2 also showed a two-step reduction (at 364 and 480 °C) and the ratio of the lower temperature peak to the higher temperature peak was around 2. The lower temperature reduction was attributed to the reduction of MnO_2 to Mn_3O_4 and the higher temperature peak was attributed to the reduction of Mn_3O_4 to MnO. Similar reduction profiles were previously observed for γ- and β-MnO_2 which support our assignments.[15] When mesoporous and nonporous manganese

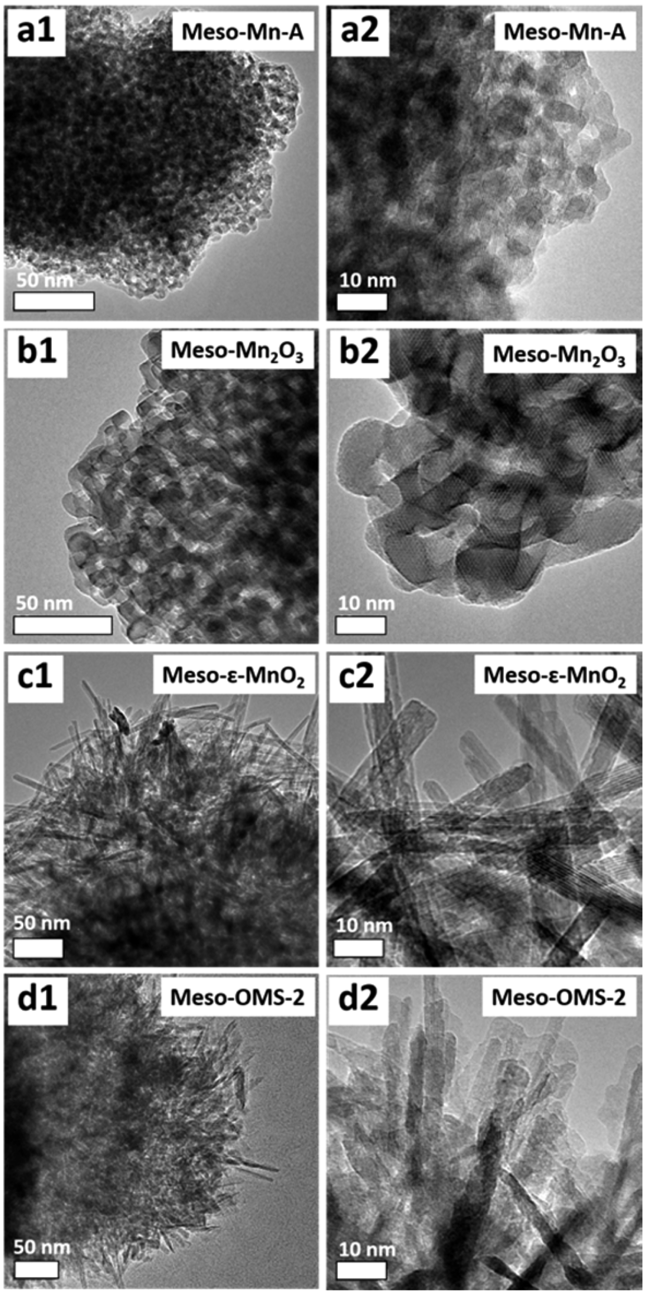

Figure 2. HR-TEM images of mesoporous manganese oxides. (a) Meso-Mn-A (scale bars are 50 nm at a1 and 10 nm at a2), (b) Meso-Mn_2O_3 (scale bars are 50 nm at b1 and 10 nm at b2), (c) Meso- ε-MnO_2 (scale bars are 50 nm at c1 and 10 nm at c2), and (d) Meso-OMS-2 (scale bars are 50 nm at d1 and 10 nm at d2).

oxides are compared based on their lowest temperature reduction peaks, the enhanced reducibility of the samples is in the order C-Mn_2O_3 < R-OMS-2 < Meso-Mn_2O_3 < Meso-OMS-2 < Meso-ε-MnO_2 < Meso-Mn-A.

The catalytic oxidation of CO on various manganese oxides have been extensively studied and thought to be happening through a Mars-van-Krevelen reaction mechanism.[15,36,37] According to the Mars-van-Krevelen mechanism, the surface adsorbed CO is reacted with labile lattice oxygen to form CO_2 (equation S4 in the Supporting Information).[36,37] The catalytic activity of mesoporous manganese oxides for CO oxidation was reported in Figure 3b and T_{100} (100% conversion) temperatures are listed in Table 1. Meso-Mn-A showed the highest activity (100% conversion at RT). Meso-ε-MnO_2 and Meso-OMS-2 demonstrated similar activity and both reached 100% conversions at 50 °C. However, Meso-ε-MnO_2 was slightly more active than Meso-OMS-2, which showed 95% (vs 60%) conversion at RT. Meso-Mn_2O_3 showed the lowest activity among the mesoporous manganese oxides and 100% conversion was observed at 75 °C. All mesoporous manganese oxides were much more active than nonporous manganese oxides (R-OMS-2 and C-Mn_2O_3). R-OMS-2 reached 100% conversion at 225 °C and C−Mn_2O_3 only reached 20% conversion at the same temperature. The order of catalytic activity was found to be the same as the order of reducibility, despite the fact that the enhanced reducibility does not always correlate with the activity in catalytic oxidation reactions (i.e., toluene, formaldehyde, and ethanol). Crystallinity, surface area, lattice oxygen mobility, and sorption of reactants and products are some of the most important parameters determining the activity of a redox catalyst.[15,36,37] Crystalline mesoporous

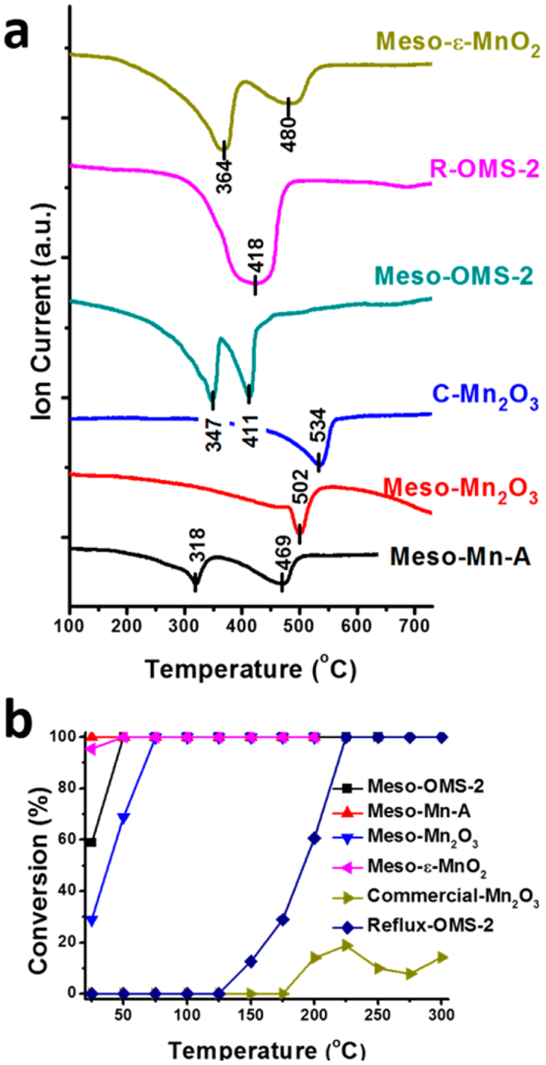

Figure 3. (a) H_2-TPR (temperature-programming reduction) profiles of mesoporous manganese oxides (Meso-Mn-A, Meso-Mn_2O_3, Meso-ε-MnO_2, and Meso-OMS-2), C-Mn_2O_3, and R-OMS-2 samples. (b) The catalytic performance of mesoporous manganese oxides, C-Mn_2O_3, and Reflux-OMS-2 samples for catalytic oxidation of CO (2% O_2 + 1% CO balanced in N_2). The flow rate is 20 sccm.

manganese oxides have similar structural properties (high surface area, monomodal mesoporosity, and high mesopore volume), because all crystalline mesoporous samples were synthesized from the same starting material (Meso-Mn-A). Moreover, both $Mn^{2+/3+}$ (i.e., Mn_2O_3) and $Mn^{4+/3+}$ (i.e., MnO_2) redox reactions are known to show catalytic activity for CO oxidation (seeequation S4 in the Supporting Information). Therefore, we attributed the order of catalytic activity of mesoporous manganese oxides for CO oxidation to the order of ease of reducibility. The ε-MnO_2 phase (Meso-ε-MnO_2) was found to be the most active phase among the crystalline samples. Therefore, Meso-ε-MnO_2 was also used for the catalytic stability tests (see Figure S6 in the Supporting Information) and no activity loss was observed for CO oxidation after 24 h of reaction.

In summary, amorphous mesoporous manganese oxide was transformed into two different crystalline phases (OMS-2 and ε-MnO_2) of manganese oxide under mild acidic conditions (0.5 M), at low temperatures (70 °C), and in very short times (2 h). The materials maintained high surface areas (≥ 196 m^2/g) and mesoporosity (4.8−5.6 nm) after the transformation. Nanocrystalline mesoporous manganese oxides demonstrated enhanced reducibility and high catalytic activity for CO oxidation. The catalytic activity correlated with the reducibility and followed the order C-Mn_2O_3 < R-OMS-2 < Meso-Mn_2O_3 < Meso-OMS-2 < Meso-ε-MnO_2 < Meso-Mn-A. Extension of this work describing the synthesis of various polymorphs (α-, β-, γ-) of MnO_2 and OMS materials is underway.

■ ASSOCIATED CONTENT

Ⓢ Supporting Information

The list of chemicals, detailed experimental procedures for the synthesis of mesoporous manganese oxides, details for materials characterization. This material is available free of charge via the Internet at http://pubs.acs.org.

■ AUTHOR INFORMATION

Corresponding Author

*E-mail: steven.suib@uconn.edu.

Author Contributions

A.S.P. designed, synthesized, and characterized the materials. W.S. and A.S.P. performed the catalytic reactions. D.K. performed H_2-TPR experiments. C.H.K. and M.S.S. collected the electron microscopy images. A.S.P. and S.L.S. wrote the manuscript.

Funding

This work was funded by the U.S. Department of Energy, Office of Basic Energy Sciences, Division of Chemical, Biological and Geological Sciences, under Grant DE-FG02−86ER13622.A000.

Notes

The authors declare no competing financial interest.

■ REFERENCES

(1) Poyraz, A. S.; Biswas, S.; Genuino, H. C.; Dharmarathna, S.; Kuo, C.-H.; Suib, S. L. Bimodification of Mesoporous Silicon Oxide by Coupled “In Situ Oxidation at the Interface and Ion Exchange” and its Catalytic Activity in the Gas-Phase Toluene Oxidation. *ChemCatChem.* **2012**, *5*, 920−930.

(2) Poyraz, A. S.; Kuo, C.-H.; Biswas, S.; King’ondu, C. K.; Suib, S. L. A General Approach to Crystalline and Monomodal Pore Size Mesoporous Materials. *Nat. Commun.* **2013**, 4.

(3) Debecker, D. P.; Hulea, V.; Mutin, P. H. Mesoporous Mixed Oxide Catalysts via Non-hydrolytic Sol−Gel: A Review. *Appl. Catal., A* **2013**, *451*, 192−206.

(4) Vos, D. E. D.; Dams, M.; Sels, B. F.; Jacobs, P. A. Ordered Mesoporous and Microporous Molecular Sieves Functionalized with Transition Metal Complexes as Catalysts for Selective Organic Transformations. *Chem. Rev.* **2002**, *102*, 3615−3640.

(5) Walcarius, A. Mesoporous Materials and Electrochemistry. *Chem. Soc. Rev.* **2013**, *42*, 4098.

(6) Taguchi, A.; Schüth, F. Ordered Mesoporous Materials in Catalysis. *Microporous Mesoporous Mater.* **2005**, *77*, 1−45.

(7) Ren, Y.; Ma, Z.; Bruce, P. G. Ordered Mesoporous Metal Oxides: Synthesis and Applications. *Chem. Soc. Rev.* **2012**, *41*, 4909.

(8) Bibby, A.; Mercier, L. Adsorption and Separation of Water-Soluble Aromatic Molecules by Cyclodextrin-Functionalized Mesoporous Silica. *Green Chem.* **2003**, *5*, 15−19.

(9) Wu, Z.; Zhao, D. Ordered Mesoporous Materials as Adsorbents. *Chem. Commun.* **2011**, *47*, 3332−3338.

(10) Brezesinski, T.; Wang, J.; Tolbert, S. H.; Dunn, B. Ordered Mesoporous α-MoO_3 with Iso-oriented Nanocrystalline Walls for Thin-Film Pseudocapacitors. *Nat. Mater.* **2010**, *9*, 146−151.

(11) Sinha, A. K.; Suzuki, K.; Takahara, M.; Azuma, H.; Nonaka, T.; Suzuki, N.; Takahashi, N. Preparation and Characterization of Mesostructured γ-Manganese Oxide and Its Application to VOCs Elimination. *J. Phys. Chem. C* **2008**, *112*, 16028−16035.

(12) Tian, Z.-R.; Tong, W.; Wang, J.-Y.; Duan, N.-G.; Krishnan, V. V.; Suib, S. L. Manganese Oxide Mesoporous Structures: Mixed-Valent Semiconducting Catalysts. *Science* **1997**, *276*, 926−930.

(13) Jiao, F.; Bruce, P. G. Two- and Three-Dimensional Mesoporous Iron Oxides with Microporous Walls. *Angew. Chem.* **2004**, *116*, 6084−6087.

(14) Sinha, A. K.; Suzuki, K. Three-Dimensional Mesoporous Chromium Oxide: A Highly Efficient Material for the Elimination of Volatile Organic Compounds. *Angew. Chem.* **2005**, *117*, 275−277.

(15) Liang, S.; Teng, F.; Bulgan, G.; Zong, R.; Zhu, Y. J. Effect of Phase Structure of MnO_2 Nanorod Catalyst on the Activity for CO Oxidation. J. *Phys. Chem. C* **2008**, *112*, 5307−5315.

(16) Takeuchi, K. J.; Yau, S. Z.; Menard, M. C.; Marschilok, A. C.; Takeuchi, E. S. Synthetic Control of Composition and Crystallite Size of Silver Hollandite, $Ag_xMn_8O_{16}$: Impact on Electrochemistry. *ACS Appl. Mater. & Interfaces* **2012**, *4*, 5547−5554.

(17) Iyer, A.; Del-Pilar, J.; King’ondu, C. K.; Kissel, E.; Garces, H. F.; Huang, H.; El-Sawy, A. M.; Dutta, P. K.; Suib, S. L. Water Oxidation Catalysis using Amorphous Manganese Oxides, Octahedral Molecular Sieves (OMS-2), and Octahedral Layered (OL-1) Manganese Oxide Structures. *J. Phys. Chem. C* **2012**, *116*, 6474−6483.

(18) Zhang, C.; Feng, C.; Zhang, P.; Guo, Z.; Chen, Z.; Li, S.; Liu, H. $K_{0.25}Mn_2O_4$ Nanofiber Microclusters as High Power Cathode Materials for Rechargeable Lithium Batteries. *RSC Adv.* **2012**, *2*, 1643.

(19) Li, J.; Wang, R.; Hao, J. Role of Lattice Oxygen and Lewis Acid on Ethanol Oxidation over OMS-2 Catalyst. *J. Phys. Chem. C* **2010**, *114*, 10544−10550.

(20) Xia, Y.; Dai, H.; Jiang, H.; Zhang, L. Three-dimensional Ordered Mesoporous Cobalt Oxides: Highly Active Catalysts for the Oxidation of Toluene and Methanol. *Catal. Commun.* **2010**, *11*, 1171−1175.

(21) Jiao, F.; Jumas, J.-C.; Womes, M.; Chadwick, A. V.; Harrison, A.; Bruce, P. G. Synthesis of Ordered Mesoporous Fe_3O_4 and γ-Fe_2O_3 with Crystalline Walls Using Post-Template Reduction/Oxidation. *J. Am. Chem. Soc.* **2006**, *128*, 12905−12909.

(22) Wang, X.; Li, Y. Synthesis and Formation Mechanism of Manganese Dioxide Nanowires/Nanorods. *Chem. - Eur. J.* **2003**, *9*, 300−306.

(23) Ding, Y.-S.; Shen, X.-F.; Gomez, S.; Luo, H.; Aindow, M.; Suib, S. L. Hydrothermal Growth of Manganese Dioxide into Three-Dimensional Hierarchical Nanoarchitectures. *Adv. Funct. Mater.* **2006**, *16*, 549−555.

(24) Liu, Y.; Wang, H.; Zhu, Y.; Wang, X.; Liu, X.; Li, H.; Qian, Y. Pyrolysis Synthesis of Magnetic @e- and @b-MnO_2 Nanostructures

and the Polymorph Discrimination. *Solid State Commun.* **2009**, *149*, 1514−1518.

(25) Suib, S. L. Porous Manganese Oxide Octahedral Molecular Sieves and Octahedral Layered Materials. *Acc. Chem. Res.* **2008**, *41*, 479−487.

(26) Du, Y.; Meng, Q.; Wang, J.; Yan, J.; Fan, H.; Liu, Y.; Dai, H. Three-dimensional Mesoporous Manganese Oxides and Cobalt Oxides: High-efficiency Catalysts for the Removal of Toluene and Carbon Monoxide. *Microporous Mesoporous Mater.* **2012**, *162*, 199−206.

(27) Poyraz, A. S.; Hines, W. A.; Kuo, C.-H.; Li, N.; Perry, D. M.; Suib, S. L. Mesoporous Co_3O_4 Nanostructured Material Synthesized by One-Step Soft-Templating: A magnetic study. *J. Appl. Phys.* **2014**, *115*, 114309.

(28) Ghodbane, O.; Pascal, J.-L.; Favier, F. Microstructural Effects on Charge-Storage Properties in MnO_2-Based Electrochemical Supercapacitors. *ACS Appl. Mater. Interfaces* **2009**, *1*, 1130−1139.

(29) Wang, Y.; Kobayashi, H.; Yamaguchi, K.; Mizuno, N. Manganese Oxide Catalyzed Transformation of Primary Amines to Primary Amides Through the Sequence of Oxidative Dehydrogenation and Successive Hydration. *Chem. Commun.* **2012**, *48*, 2642.

(30) Luo, J.; Zhang, Q.; Garcia-Martinez, J.; Suib, S. L. Adsorptive and Acidic Properties, Reversible Lattice Oxygen Evolution, and Catalytic Mechanism of Cryptomelane-Type Manganese Oxides as Oxidation Catalysts. *J. Am. Chem. Soc.* **2008**, *130*, 3198−3207.

(31) Artamonova, I. V.; Gorichev, I. G.; Godunov, E. B. Kinetics of Manganese Oxides Dissolution in Sulphuric Acid Solutions Containing Oxalic Acid. *Engineering* **2013**, *05*, 714−719.

(32) Walanda, D. K.; Lawrance, G. A.; Donne, S. W. Hydrothermal MnO_2: Synthesis, Structure, Morphology and Discharge Performance. *J. Power Sources* **2005**, *139*, 325−341.

(33) Sinha, A. K.; Suzuki, K.; Takahara, M.; Azuma, H.; Nonaka, T.; Fukumoto, K. Mesostructured Manganese Oxide/Gold Nanoparticle Composites for Extensive Air Purification. *Angew. Chem., Int. Ed.* **2007**, *46*, 2891−2894.

(34) Luo, J.-Y.; Meng, M.; Li, X.; Li, X.-G.; Zha, Y.-Q.; Hu, T.-D.; Xie, Y.-N.; Zhang, J. Mesoporous $Co_3O_4-CeO_2$ and $Pd/Co_3O_4-CeO_2$ Catalysts: Synthesis, Characterization and Mechanistic Study of Their Catalytic Properties for Low-Temperature CO Oxidation. *J. Catal.* **2008**, *254*, 310−321.

(35) Chen, T.; Dou, H.; Li, X.; Tang, X.; Li, J.; Hao, J. Tunnel Structure Effect of Manganese Oxides in Complete Oxidation of Formaldehyde. *Microporous Mesoporous Mater.* **2009**, *122*, 270−274.

(36) Ramesh, K.; Chen, L.; Chen, F.; Liu, Y.; Wang, Z.; Han, Y. Re-investigation, the CO Oxidation Mechanism Over Unsupported MnO, Mn_2O_3, and MnO_2 Catalysts. *Catal. Today* **2008**, *131*, 477−482.

(37) Ozacar, M.; Poyraz, A. S.; Genuino, H. C.; Kuo, C.; Meng, Y.; Suib, S. L. Influence of Silver on the Catalytic Properties of the Cryptomelane and Ag-Hollandite types manganese oxides OMS-2 in the Low-Temperature CO Oxidation. *Appl. Catal., A* **2013**, *462−463*, 64−74.

(38) Lin, R.; Liu, W.; Zhang, Y.; Luo, M. CO Oxidation Activity and TPR Characterization of Ag-Mn Complex Oxide Catalysts. *React. Kinet. Catal. Lett.* **2001**, *72*, 289−295.